Electronic Supplementary Information

Effects of Mixing between Short-chain and Branched-chain Alcohols in Protonated Clusters

Po-Jen Hsu,[*1] Takahiro Shinkai, [2] Pei-Han Tai,[3] Asuka Fujii,[*2] Jer-Lai Kuo[*1]

[1]Institute of Atomic and Molecular Sciences, Academia Sinica, Taipei 10617, Taiwan.

[2]Department of Chemistry, Graduate School of Science, Tohoku University, Sendai 980-8578, Japan.

[3]Department of Chemistry, National Taiwan Normal University, Taipei 106, Taiwan.

* Corresponding authors: pjhsu@gate.sinica.edu.tw (P.-J.H), asuka.fujii.c5@tohoku.ac.jp (A.F.), jlkuo@pub.iams.sinica.edu.tw (J.-L.K)

Contents

the B3LYP and B3LYP+D3 level of theories.

Figure S2 Temperature-dependent relative population of $H^+(MeOH)_m(t\text{-}BuOH)_t$ for $m + t = 4$ by Q-HSA.

Figures S3-S7 Simulated IR spectra of $H^+(MeOH)_m(t\text{-}BuOH)_t$ for $m + t = 4$.

Figure S8 Relative zero-point corrected energies of $H^+(MeOH)_m(t\text{-}BuOH)_t$ for $m + t = 5$ optimized by the B3LYP and B3LYP+D3 level of theories.

Figure S9 Temperature-dependent relative population of $H^+(MeOH)_m(t\text{-}BuOH)_t$ for $m + t = 5$ by Q-HSA.

Figures S10-S15 Simulated IR spectra of $H^+(MeOH)_m(t\text{-}BuOH)_t$ for $m + t = 5$.

Figure S16 Comparisons of the observed and the simulated IR spectra by removing the lowest energy structures for $(m, t) = (4, 1)$ and $(1, 4)$.

Figure S17 Dissociation energies of $H^+(MeOH)_m(t\text{-}BuOH)_t$, $m + t = 5$ with a note on the artificial discrimination of specific isomers in dissociation spectroscopy

Table S1 Number of isomers from the random structural search of $H^+(MeOH)_m(t\text{-}BuOH)_t$ for $m + t = 4$. The indices m and t refer to the number of methanol and *tert*-butyl alcohol molecules in $H^+(MeOH)_m(t\text{-}BuOH)_t$ mixed clusters.

$H^+(MeOH)_m(t\text{-}BuOH)_t$ (m, t)			(4, 0)	(3, 1)	(2, 2)	(1, 3)	(0, 4)
B3LYP/ 6-31+G*	**L**	$t\text{-}BuOH_2^+$	-	28	97	132	20
		$MeOH_2$	19	53	54	-	-
	C	$t\text{-}BuOH_2^+$	-	2	4	4	3
		$MeOH_2$	2	4	4	3	-
B3LYP-D3/ 6-31+G*	**L**	$t\text{-}BuOH_2^+$	-	41	178	232	70
		$MeOH_2$	42	86	82	-	-
	C	$t\text{-}BuOH_2^+$	-	4	14	17	4
		$MeOH_2$	2	8	13	4	-

Table S2 Number of isomers from the random structural search of $H^+(MeOH)_m(t\text{-}BuOH)_t$ for $m + t = 5$. The indices m and t refer to the number of methanol and *tert*-butyl alcohol molecules in $H^+(MeOH)_m(t\text{-}BuOH)_t$ mixed clusters.

$H^+(MeOH)_m(t\text{-}BuOH)_t$ (m, t)			(5, 0)	(4, 1)	(3, 2)	(2, 3)	(1, 4)	(0, 5)
B3LYP/ 6-31+G*	L	$t\text{-}BuOH_2^+$	-	50	145	286	165	28
		$MeOH_2$	23	59	56	22	20	-
	C	$t\text{-}BuOH_2^+$	-	4	12	21	18	8
		$MeOH_2$	4	6	3	3	-	-
	Ct	$t\text{-}BuOH_2^+$	-	8	22	20	20	9
		$MeOH_2$	2	2	2	-	-	-
B3LYP-D3/ 6-31+G*	L	$t\text{-}BuOH_2^+$	-	59	156	373	292	77
		$MeOH_2$	25	55	46	44	31	-
	C	$t\text{-}BuOH_2^+$	-	6	21	31	24	11
		$MeOH_2$	3	6	6	5	-	-
	Ct	$t\text{-}BuOH_2^+$	-	9	30	28	41	13
		$MeOH_2$	2	2	5	2	1	-

Table S3 Electronic (E_0) and zero-point corrected (E_0+E_{zpe}) energies (in Hartree) of the four lowest energy structures in B3LYP calculations of (*m, t*) = (4, 1) and B3LYP+D3 calculations of (*m, t*) = (1, 4). Geometric optimization and frequency analysis with MP2/aug-cc-pVDZ were applied for (*m, t*) = (4, 1). For (*m, t*) = (1, 4), only single point calculations were done. The preferential type of isomers observed in the experimental measurement is marked by *. Note that E_0 of (fM, pT, C) in red color is the lowest among the four (4, 1) structures. When taking the zero-point energy into account (E_0+E_{zpe}), it becomes the second lowest energy.

(*m, t*) = (4, 1)	B3LYP/6-31+G(d) **E_0**	B3LYP/6-31+G(d) **E_0+E_{zpe}**	MP2/aug-cc-pVDZ **E_0**	MP2/aug-cc-pVDZ **E_0+E_{zpe}**
1: (fT, pM, **C**)	-697.022403	-696.660506	-695.140287	-694.778538
2: (fM, pT, **Ct**)	-697.023804	-696.660245	-695.140738	-694.777551
***3: (fM, pT, C**)	-697.023445	-696.660242	-695.140974	-694.778330
4: (fM, pT, **Ct**)	-697.023907	-696.660160	-695.140204	-694.777287
(*m, t*) = (1, 4)	B3LYP+D3/6-31+G(d) **E_0**	B3LYP+D3/6-31+G(d) **E_0+E_{zpe}**	MP2/aug-cc-pVDZ **E_0**	MP2/aug-cc-pVDZ **E_0+E_{zpe}**
1: (fM, pT, **Ct**)	-1050.980414	-1050.361153	-1047.910353	-
2: (fT, pT, **Ct**)	-1050.978944	-1050.360487	-1047.907904	-
***3: (fT, pT, C)**	-1050.977431	-1050.360358	-1047.907028	-
4: (fT, pT, **Ct**)	-1050.978202	-1050.359987	-1047.906995	-

Table S4 The zero-point corrected global minimum energies of $m + t = 4$ and the corresponding free OH species, ion core species, and the H-bond networks.

(m, t)	$E_{global}(B3LYP)$, global minimum E	$E_{global}(B3LYP + D3)$, global minimum E
(4, 0)	-463.089126 (fM, pM, **L**)	-463.102462 (fM, pM, **C**)
(3, 1)	-580.966177 (fM, pT, **C**)	-580.994515 (fM, pT, **C**)
(2, 2)	-698.843406 (fT, pT, **C**)	-698.884914 (fT, pT, **C**)
(1, 3)	-816.71821 (fT, pT, **C**)	-816.773622 (fT, pT, **C**)
(0, 4)	-934.592414 (fT, pT, **C**)	-934.66274 (fT, pT, **C**)

Table S5 The zero-point corrected global minimum energies in Hartree and the corresponding free OH species, ion core species, and the H-bond networks for $m + t = 5$.

(m, t)	$E_{global}(B3LYP)$, global minimum E	$E_{global}(B3LYP + D3)$, global minimum E
(5, 0)	-578.784315 (fM, pM, **C**)	-578.804408 (fM, pM, **C**)
(4, 1)	-696.660507 (fT, pM, **C**)	-696.694163 (fT, pM, **C**)
(3, 2)	-814.53691 (fT, pT, **C**)	-814.583764 (fT, pT, **C**)
(2, 3)	-932.411194 (fT, pT, **C**)	-932.472998 (fT, pT, **C**)
(1, 4)	-1050.284731 (fT, pT, **Ct**)	-1050.361153 (fM, pT, **Ct**)
(0, 5)	-1168.155201 (fT, pT, **Ct**)	-1168.24787 (fT, pT, **Ct**)

Table S6 The dissociation energies of the global minima of $m + t = 5$ clusters listed in Table S5 in Hartree.

E_{dm} is the dissociation energy to the (m, t) to (m-1, t) channel, and E_{dt} is the dissociation energy for the (m, t) to (m, t-1) channel. Here, only the dissociation to the global minimum of $m + t = 4$ listed in Table S4 is considered in each channel. $E_{dm}(m,t) = [E(m-1,t) + E_m] - E(m,t)$ for the dissociation of the one methanol-loss channel, and $E_{dt}(m,t) = [E(m,t-1) + E_t] - E(m,t)$ for the dissociation of the one t-butyl alcohol-loss channel. The energies of the monomers of methanol (E_m) and t-butanol (E_t) are as follows: E_m(B3LYP) = -115.673892, E_t(B3LYP) = -233.54820, E_m(B3LYP+D3) = -115.675059, and E_t(B3LYP+D3) = -233.558363 (Hartree).

(m, t)	$E_{dm}(B3LYP)$	$E_{dm}(B3LYP+D3)$	$E_{dt}(B3LYP)$	$E_{dt}(B3LYP+D3)$
(5, 0)	0.021297	0.026887	-	-
(4, 1)	0.020438	0.024589	0.023179	0.033338
(3, 2)	0.019612	0.023791	0.022531	0.030886
(2, 3)	0.019092	0.024317	0.019586	0.029721
(1, 4)	0.018425	0.023354	0.018319	0.029168
(0, 5)	-	-	0.014585	0.026767

Table S7 The zero-point corrected energies of the most stable **C** structures in Hartree and the corresponding free OH species, ion core species, and the H-bond networks for $m + t = 5$.

(m, t)	$E_{minC}(B3LYP)$, minimum E of **C**	$E_{minC}(B3LYP + D3)$, minimum E of **C**
(5, 0)	-578.784315 (fM, pM, **C**)	-578.804408 (fM, pM, **C**)
(4, 1)	-696.660507 (fT, pM, **C**)	-696.694163 (fT, pM, **C**)
(3, 2)	-814.53691 (fT, pT, **C**)	-814.583764 (fT, pT, **C**)
(2, 3)	-932.411194 (fT, pT, **C**)	-932.472998 (fT, pT, **C**)
(1, 4)	-1050.283633 (fT, pT, **C**)	-1050.35971 (fT, pT, **C**)
(0, 5)	No **C** structures	-1168.245969 (fT, pT, **C**)

Table S8 The dissociation energies of the most stable **C** structures listed in Table S7 for $m + t = 5$ in Hartree. E_{dm} is the dissociation energy to the (m, t) to (m-1, t) channel, and E_{dt} is the dissociation energy for the (m, t) to (m, t-1) channel. Here, only the dissociation to the global minimum of $m + t = 4$ listed in Table S4 is considered in each channel. $E_{dm}(m, t) = [E(m - 1,t) + E_m] - E(m,t)$ for the dissociation of the one methanol-loss channel, and $E_{dt}(m,t) = [E(m,t - 1) + E_t] - E(m,t)$ for the dissociation of the one t-butyl alcohol-loss channel. The energies of the monomers of methanol (E_m) and t-butanol (E_t) are as follows: E_m(B3LYP) = -115.673892, E_t(B3LYP) = -233.54820, E_m(B3LYP+D3) = -115.675059, and E_t(B3LYP+D3) = -233.558363 (Hartree).

(m, t)	$E_{dm}(B3LYP)$	$E_{dm}(B3LYP + D3)$	$E_{dt}(B3LYP)$	$E_{dt}(B3LYP + D3)$
(5, 0)	0.021297	0.026887	-	-
(4, 1)	0.020438	0.024589	0.023179	0.033338
(3, 2)	0.019612	0.023791	0.022531	0.030886
(2, 3)	0.019092	0.024317	0.019586	0.029721
(1, 4)	0.017327	0.021911	0.017221	0.027725
(0, 5)	-	-	No **C** structures	0.024866

Table S9 The zero-point corrected energies of the most stable **L** structures in Hartree and the corresponding free OH species, ion core species, and the H-bond networks for $m + t = 5$.

(m, t)	$E_{minL}(B3LYP)$, minimum E of **L**	$E_{minL}(B3LYP + D3)$, minimum E in **L**
(5, 0)	-578.781939 (fM, pM, **L**)	-578.799428 (fM, pM, **L**)
(4, 1)	-696.658325 (fM, pT, **L**)	-696.690279 (fM, pT, **L**)
(3, 2)	-814.534924 (fM, pT, **L**)	-814.578795 (fM, pT, **L**)
(2, 3)	-932.410154 (fT, pT, **L**)	-932.466962 (fM, fT, pT, **L**)
(1, 4)	-1050.283199 (fT, pT, **L**)	-1050.355246 (fT, pT, **L**)
(0, 5)	-1168.15505 (fT, pT, **L**)	-1168.24249 (fT, pT, **L**)

Table S10 The dissociation energies of the most stable **L** structures listed in Table S9 for $m + t = 5$ in Hartree. E_{dm} is the dissociation energy to the (m, t) to (m-1, t) channel, and E_{dt} is the dissociation energy for the (m, t) to (m, t-1) channel. Here, only the dissociation to the global minimum of $m + t = 4$ listed in Table S4 is considered in each channel. $E_{dm}(m,t) = [E(m-1,t) + E_m] - E(m,t)$ for the dissociation of the one methanol-loss channel, and $E_{dt}(m,t) = [E(m,t-1) + E_t] - E(m,t)$ for the dissociation of the one t-butyl alcohol-loss channel. The energies of the monomers of methanol (E_m) and t-butanol (E_t) are as follows: E_m(B3LYP) = -115.673892, E_t(B3LYP) = -233.54820, E_m(B3LYP+D3) = -115.675059, and E_t(B3LYP+D3) = -233.558363 (Hartree).

(m, t)	$E_{dm}(B3LYP)$	$E_{dm}(B3LYP+D3)$	$E_{dt}(B3LYP)$	$E_{dt}(B3LYP+D3)$
(5, 0)	0.018921	0.021907	-	-
(4, 1)	0.018256	0.020705	0.020997	0.029454
(3, 2)	0.017626	0.018822	0.020545	0.025917
(2, 3)	0.018052	0.018281	0.018546	0.023685
(1, 4)	0.016893	0.017447	0.016787	0.023261
(0, 5)	-	-	0.014434	0.021387

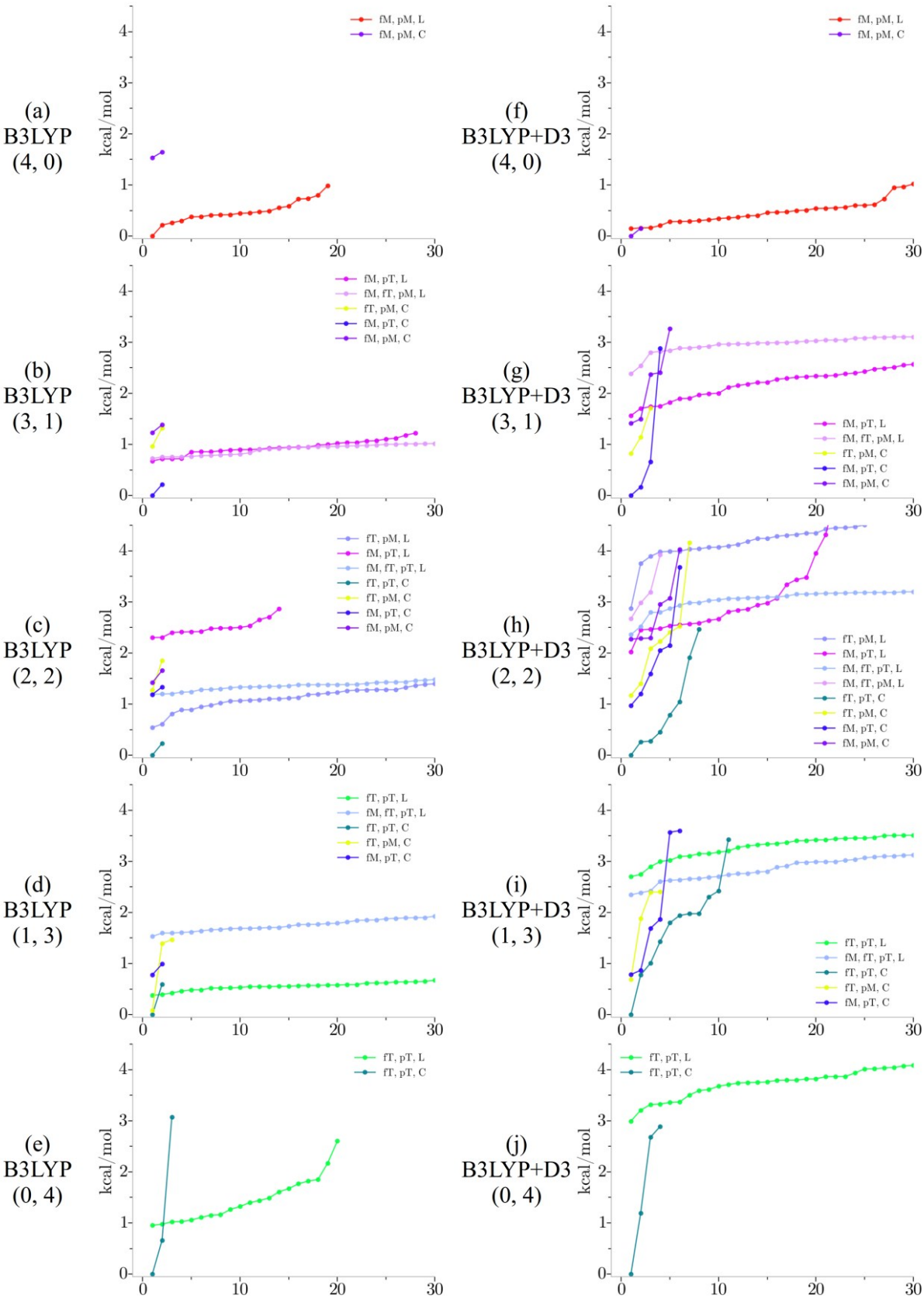

Figure S1 Relative zero-point corrected energies of $H^+(MeOH)_m(t\text{-}BuOH)_t$ clusters using the B3LYP/6-31+G* (a-e) and B3LYP/6-31+G*+D3 (f-j) level of theories for geometric optimization and frequency calculation. The abscissa is the numbering of the isomers. From top to bottom, (*m, t*) = (4, 0), (3, 1), (2, 2), (1, 3), and (0, 4). The H-bonded structures are labeled by **L** (linear) and **C** (cyclic) structures. The free OH species and the ion core are labeled by fM (free OH on methanol), fT (free OH on *tert*-butyl alcohol), pM (methanol ion core), and pT (*tert*-butyl alcohol ion core).

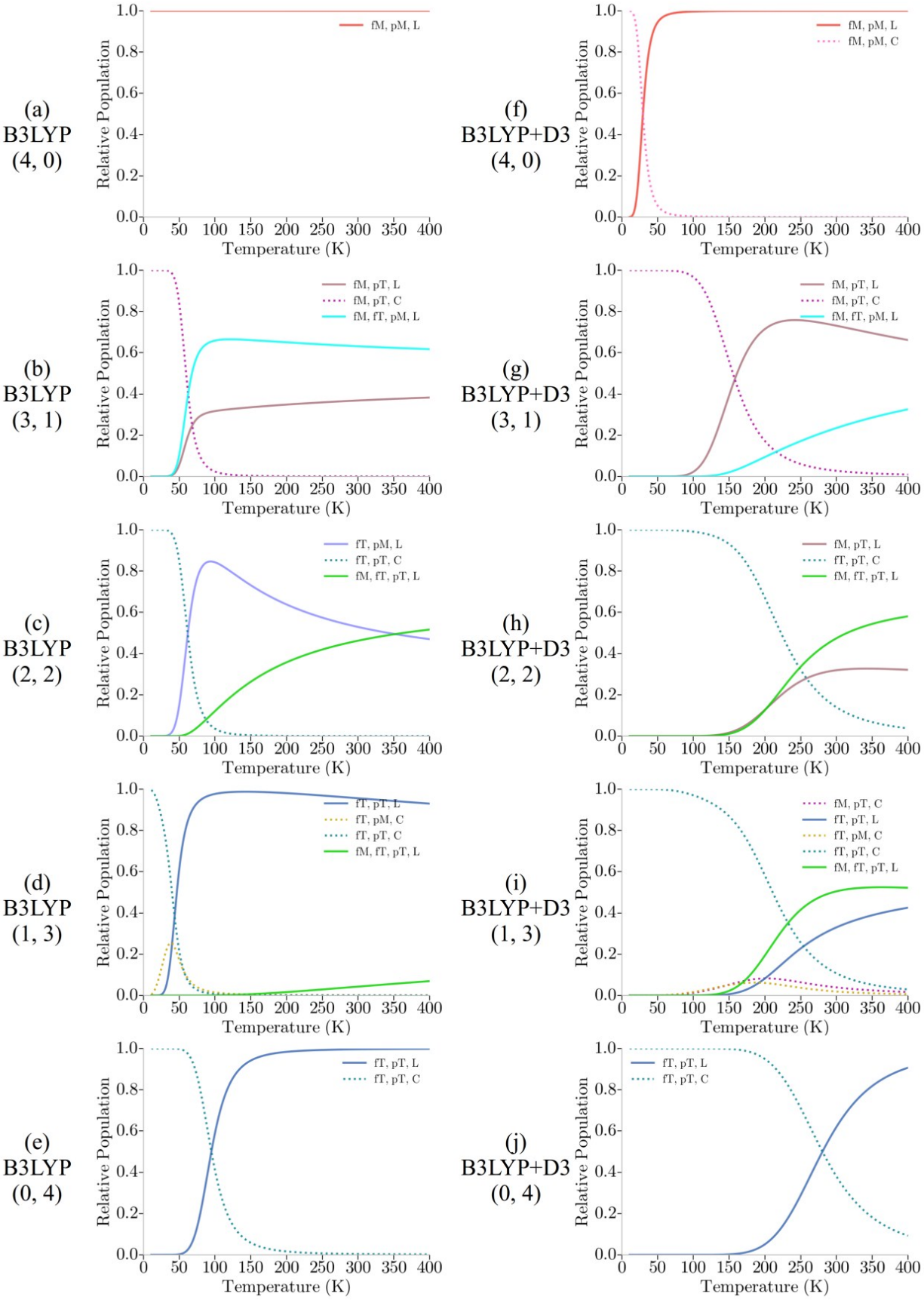

Figure S2 Temperature-dependent relative population of $H^+(MeOH)_m(t\text{-BuOH})_t$ mixed clusters using the B3LYP/6-31+G* (a-e) and B3LYP+D3/6-31+G* (f-j) level of theories for Q-HSA computation. From top to bottom, (*m, t*) = (4, 0), (3, 1), (2, 2), (1, 3), and (0, 4). The H-bonded structures are labeled by **L** (linear) and **C** (cyclic) structures. The free OH species and the ion core are labeled by fM (free OH on methanol), fT (free OH on *tert*-butyl alcohol), pM (methanol ion core), and pT (*tert*-butyl alcohol ion core).

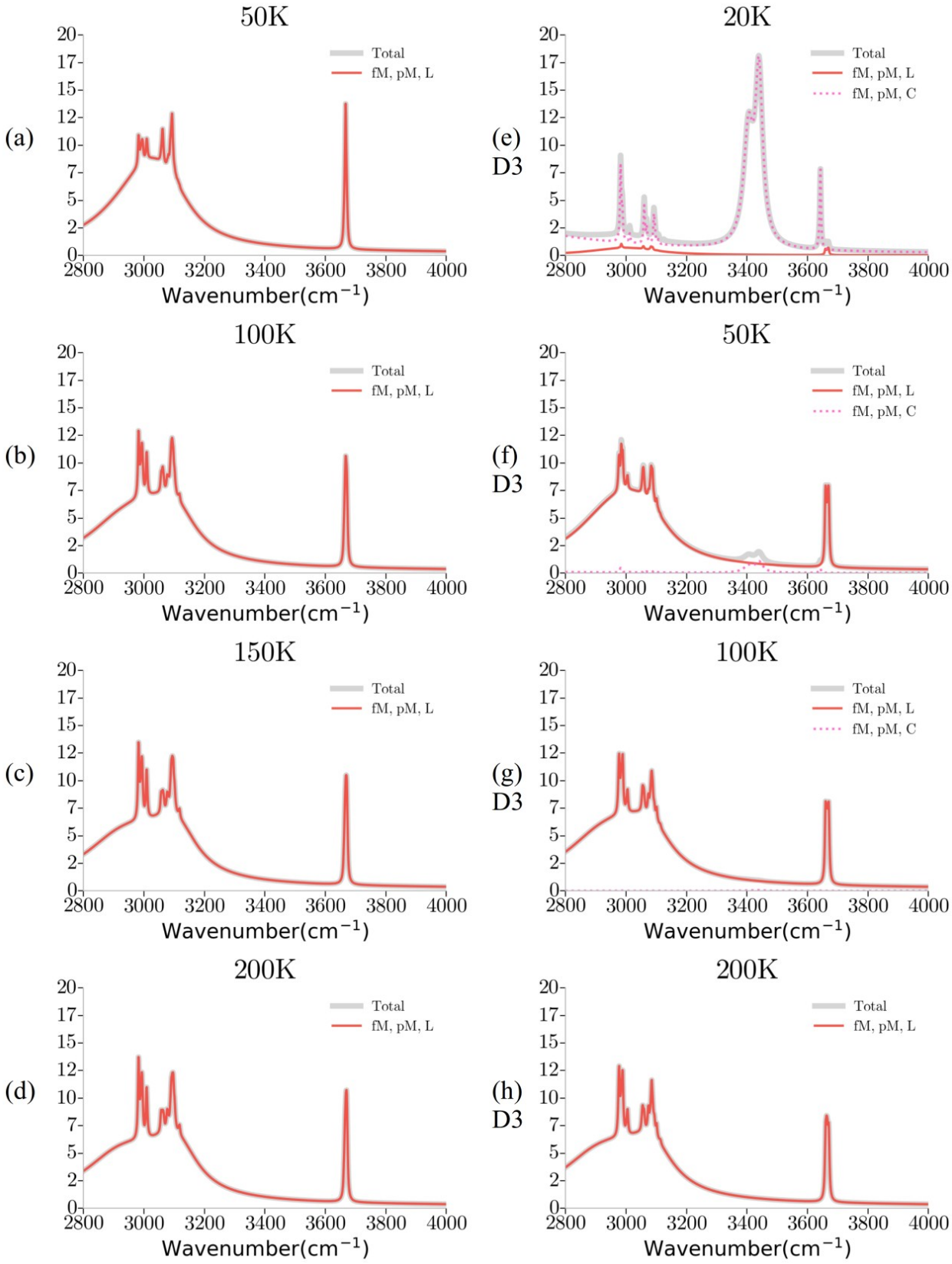

Figure S3 Simulated IR spectra of $H^+(MeOH)_4$ using the B3LYP/6-31+G* (a-d) and B3LYP+D3/6-31+G* (e-h) level of theories at various temperatures. The total spectra are marked by grey color. The H-bonded structures are labeled by **L** (linear) and **C** (cyclic) structures. The free OH species and the ion core are labeled by fM (free OH on methanol), fT (free OH on *tert*-butyl alcohol), pM (methanol ion core), and pT (*tert*-butyl alcohol ion core).

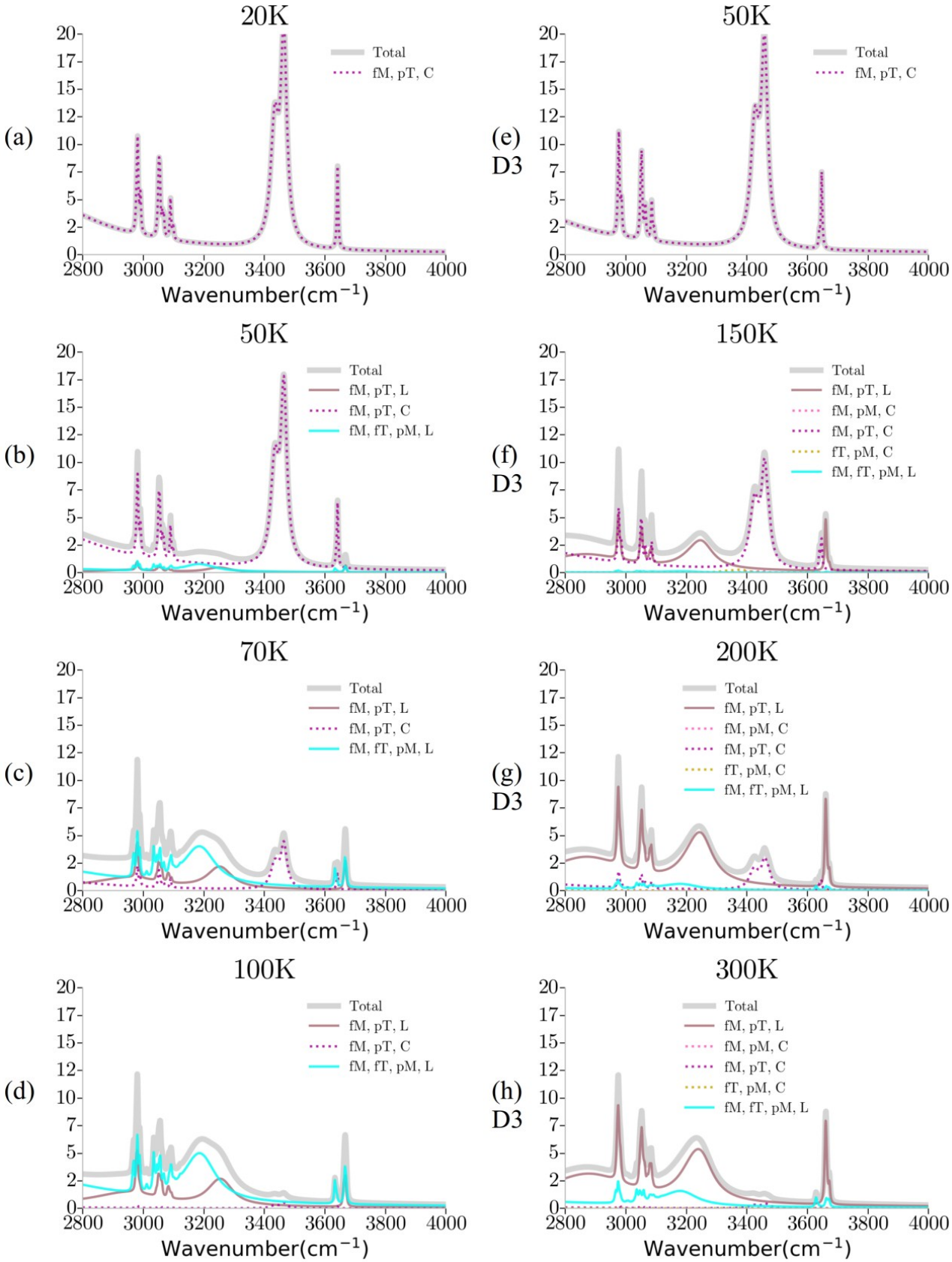

Figure S4 Simulated IR spectra of $H^+(MeOH)_3(t\text{-}BuOH)_1$ using the B3LYP/6-31+G* (a-d) and B3LYP+D3/6-31+G* (e-h) level of theories at various temperatures. The total spectra are marked by grey color. The H-bonded structures are labeled by **L** (linear) and **C** (cyclic) structures. The free OH species and the ion core are labeled by fM (free OH on methanol), fT (free OH on *tert*-butyl alcohol), pM (methanol ion core), and pT (*tert*-butyl alcohol ion core).

.

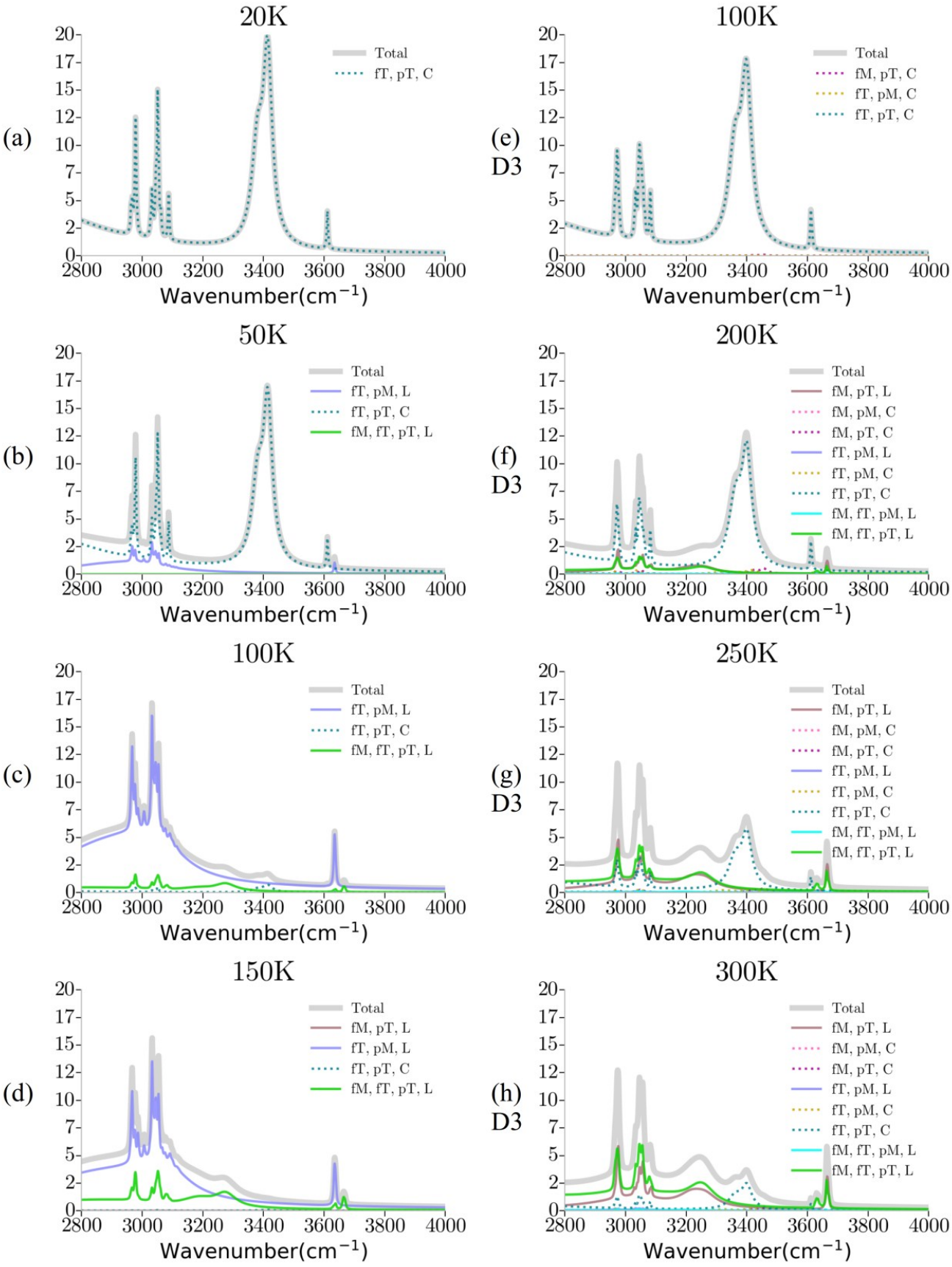

Figure S5 Simulated IR spectra of $H^+(MeOH)_2(t\text{-}BuOH)_2$ using the B3LYP/6-31+G* (a-d) and B3LYP+D3/6-31+G* (e-h) level of theories at various temperatures. The total spectra are marked by grey color. The H-bonded structures are labeled by **L** (linear) and **C** (cyclic) structures. The free OH species and the ion core are labeled by fM (free OH on methanol), fT (free OH on *tert*-butyl alcohol), pM (methanol ion core), and pT (*tert*-butyl alcohol ion core).

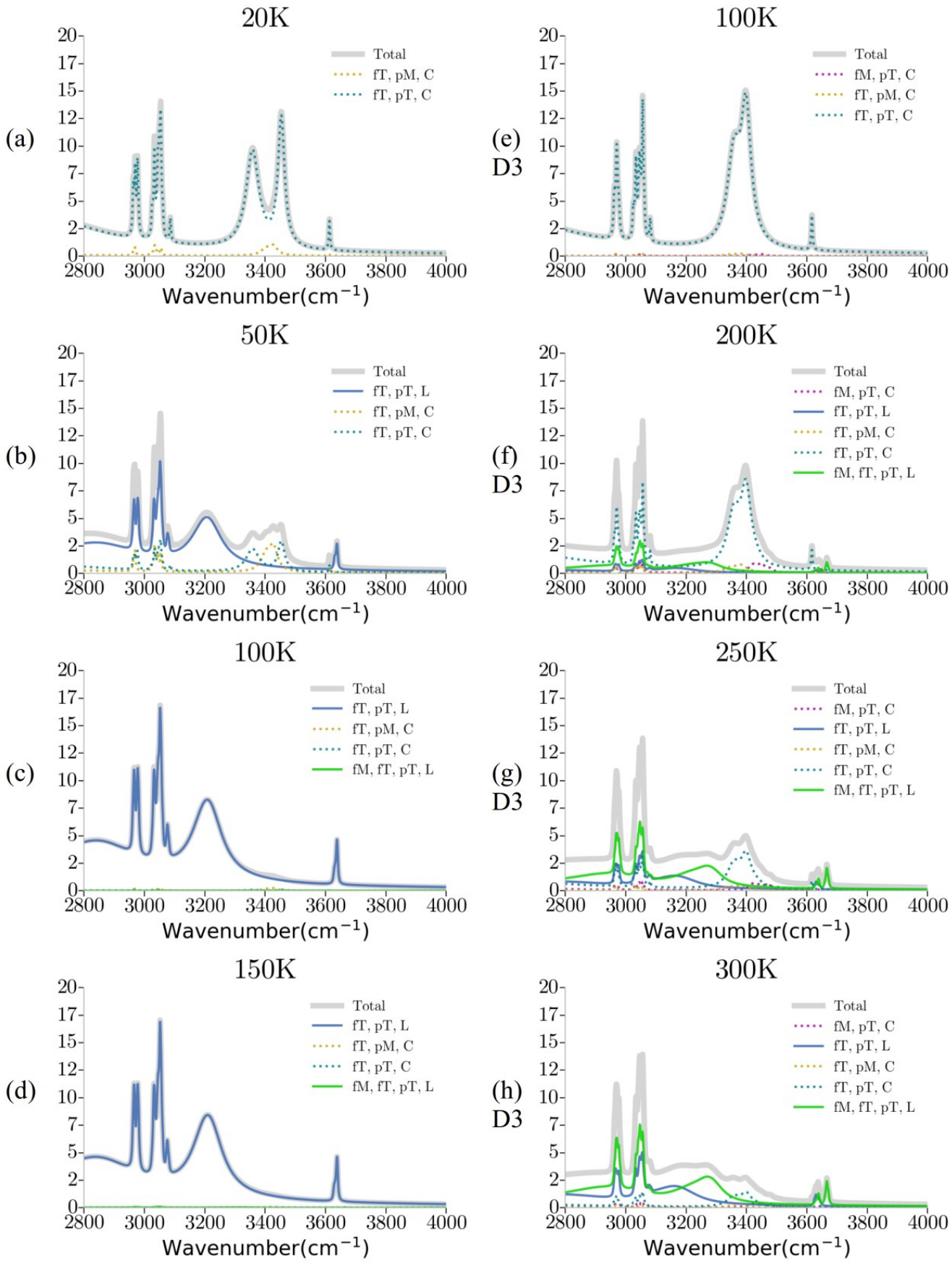

Figure S6 Simulated IR spectra of $H^+(MeOH)_1(t\text{-}BuOH)_3$ using the B3LYP/6-31+G* (a-d) and B3LYP+D3/6-31+G* (e-h) level of theories at various temperatures. The total spectra are marked by grey color. The H-bonded structures are labeled by **L** (linear) and **C** (cyclic) structures. The free OH species and the ion core are labeled by fM (free OH on methanol), fT (free OH on *tert*-butyl alcohol), pM (methanol ion core), and pT (*tert*-butyl alcohol ion core).

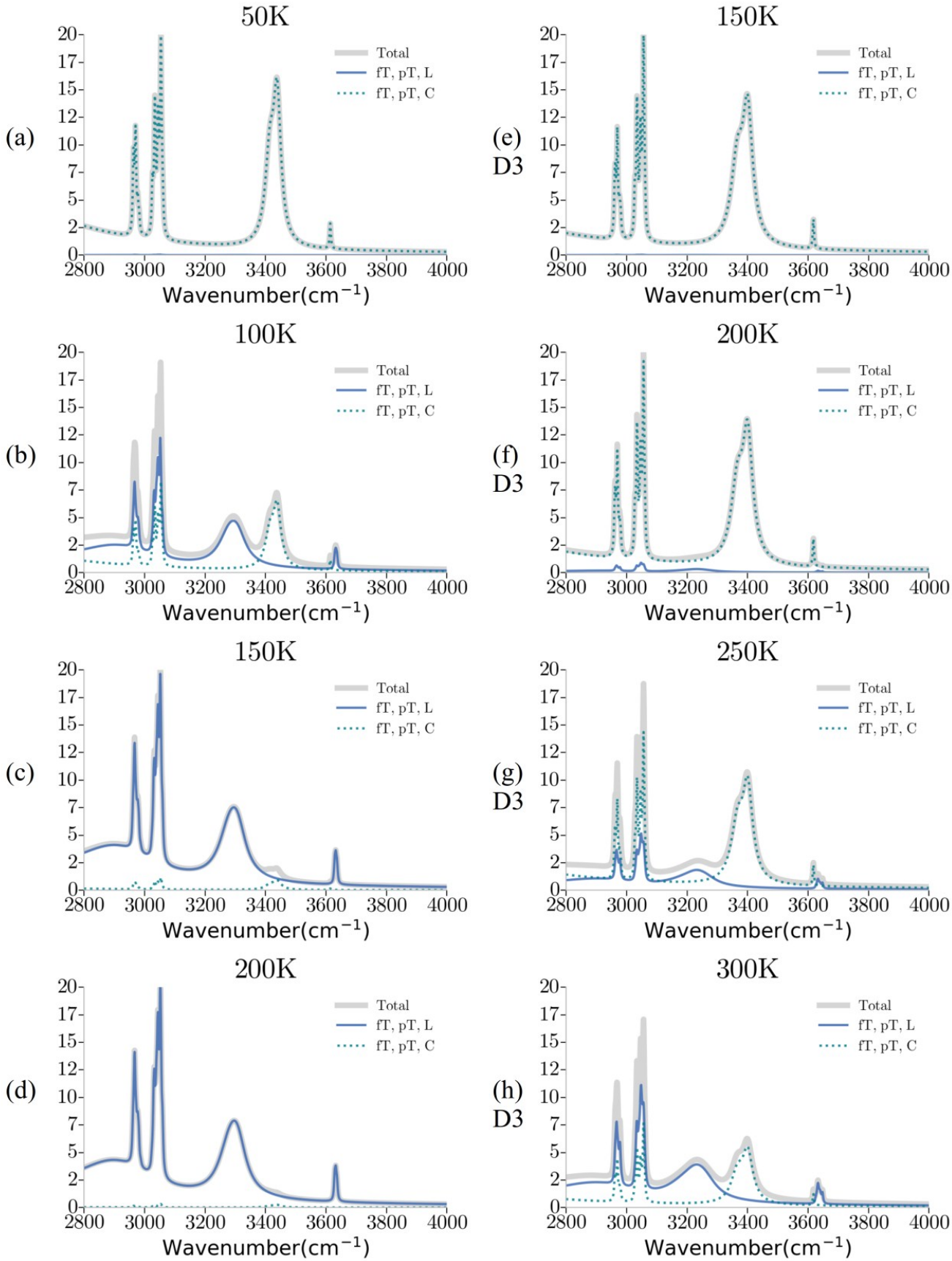

Figure S7 Simulated IR spectra of $H^+(t\text{-BuOH})_4$ using the B3LYP/6-31+G* (a-d) and B3LYP+D3/6-31+G* (e-h) level of theories at various temperatures. The total spectra are marked by grey color. The H-bonded structures are labeled by **L** (linear) and **C** (cyclic) structures. The free OH species and the ion core are labeled by fM (free OH on methanol), fT (free OH on *tert*-butyl alcohol), pM (methanol ion core), and pT (*tert*-butyl alcohol ion core).

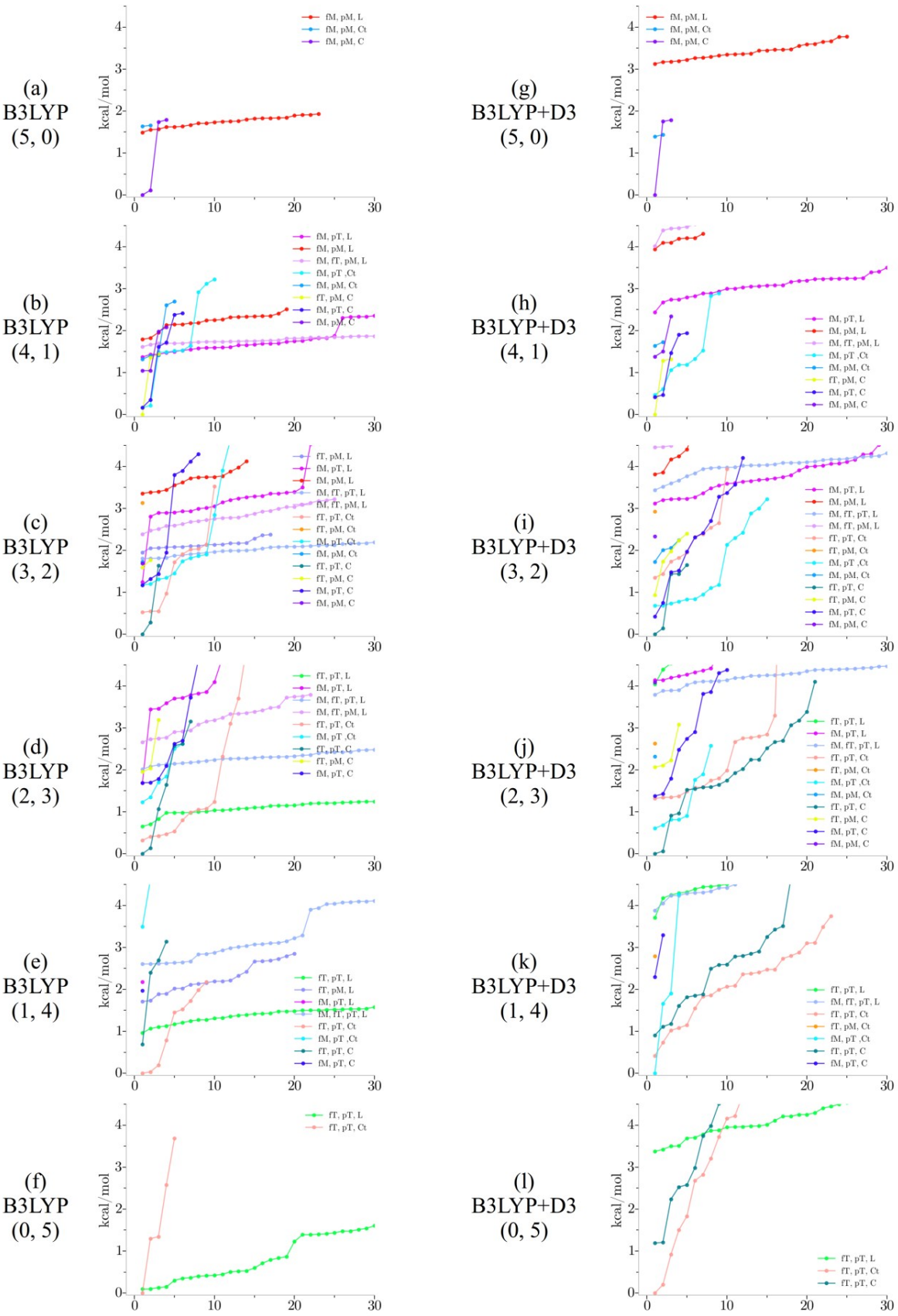

Figure S8 Relative zero-point corrected energies of $H^+(MeOH)_m(t\text{-BuOH})_t$ clusters using the B3LYP/6-31+G* (a-f) and B3LYP/6-31+G*+D3 (g-l) level of theories for geometric optimization and frequency calculation. The abscissa is the numbering of the isomers. From top to bottom, (*m, t*) = (5, 0), (4, 1), (3, 2), (2, 3) (1, 4), and (0, 5). The H-bonded structures are labeled by **L** (linear), **C** (cyclic), and **Ct** (cyclic with a tail) structures. The free OH species and the ion core are labeled by fM (free OH on methanol), fT (free OH on *tert*-butyl alcohol), pM (methanol ion core), and pT (*tert*-butyl alcohol ion core).

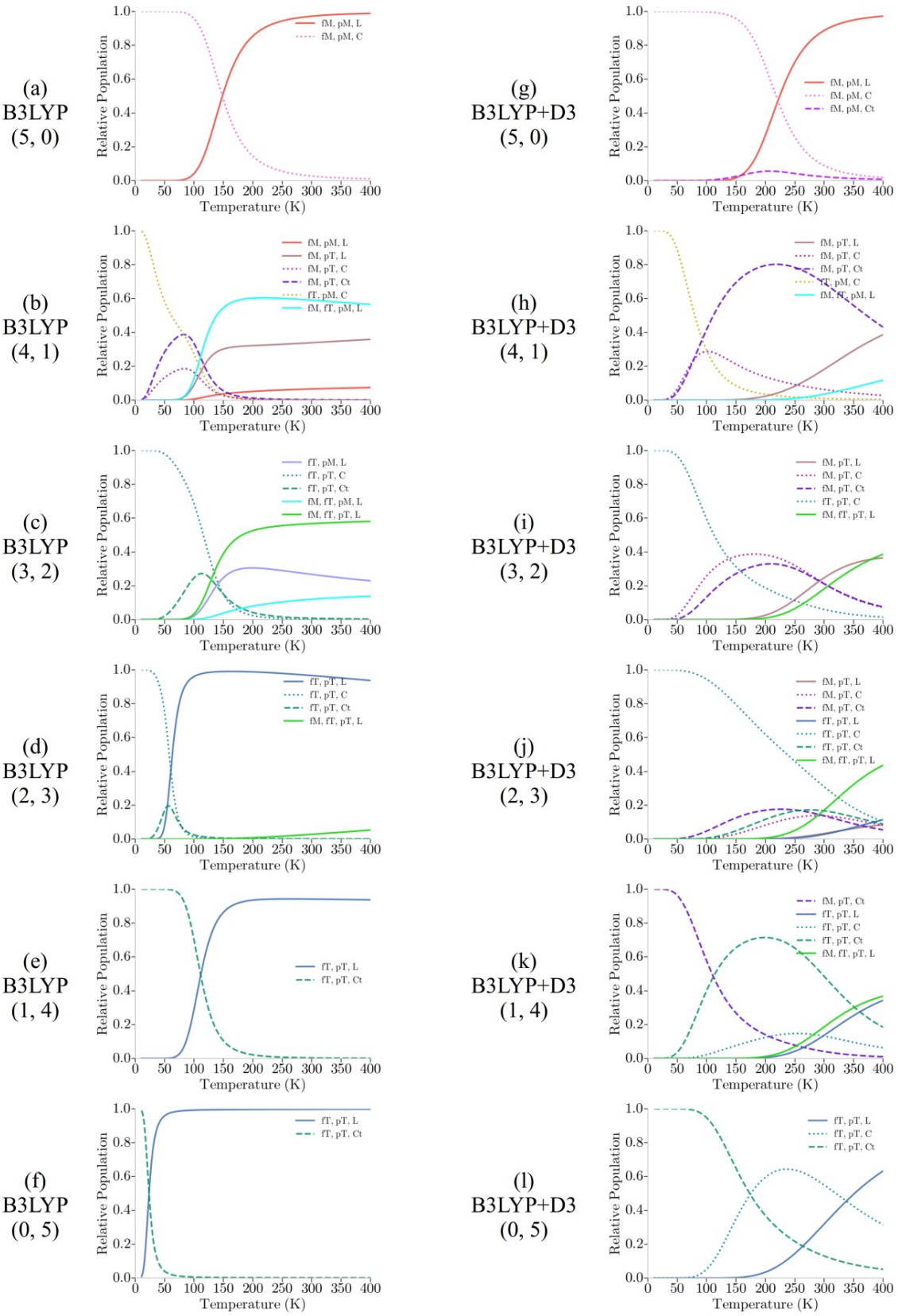

Figure S9 Temperature-dependent relative population of $H^+(MeOH)_m(t\text{-BuOH})_t$ mixed clusters using the B3LYP/6-31+G* (a-f) and B3LYP+D3/6-31+G* (g-l) level of theories for Q-HSA computation. From top to bottom, (*m, t*) = (5, 0), (4, 1), (3, 2), (2, 3), (1, 4), and (0, 5). The H-bonded structures are labeled by **L** (linear), **C** (cyclic), and **Ct** (cyclic with a tail) structures. The free OH species and the ion core are labeled by fM (free OH on methanol), fT (free OH on *tert*-butyl alcohol), pM (methanol ion core), and pT (*tert*-butyl alcohol ion core).

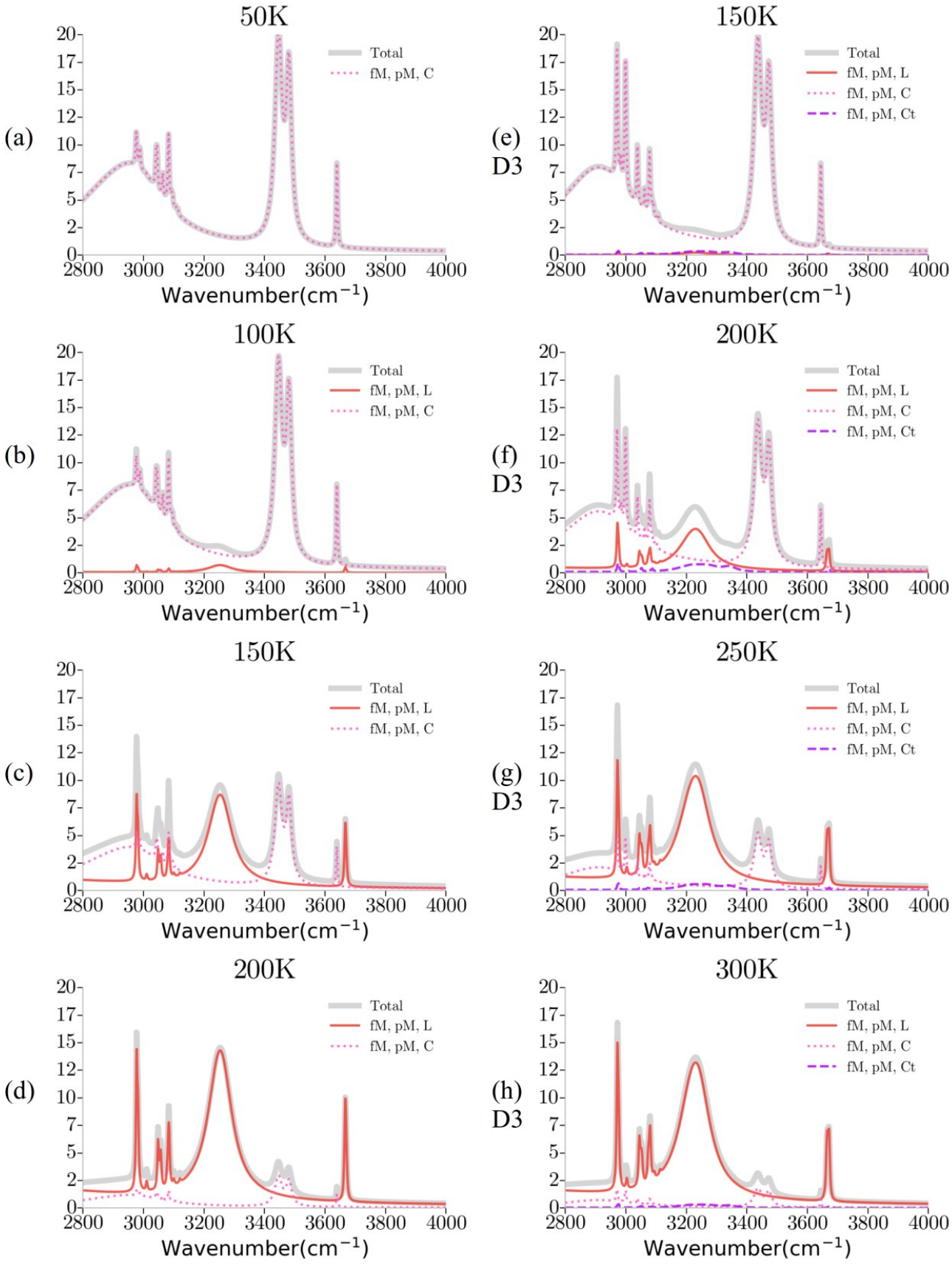

Figure S10 Simulated IR spectra of $H^+(MeOH)_5$ using the B3LYP/6-31+G* (a-d) and B3LYP+D3/6-31+G* (e-h) level of theories at various temperatures. The total spectra are marked by grey color. The H-bonded structures are labeled by **L** (linear), **C** (cyclic), and **Ct** (cyclic with a tail) structures. The free OH species and the ion core are labeled by fM (free OH on methanol), fT (free OH on *tert*-butyl alcohol), pM (methanol ion core), and pT (*tert*-butyl alcohol ion core).

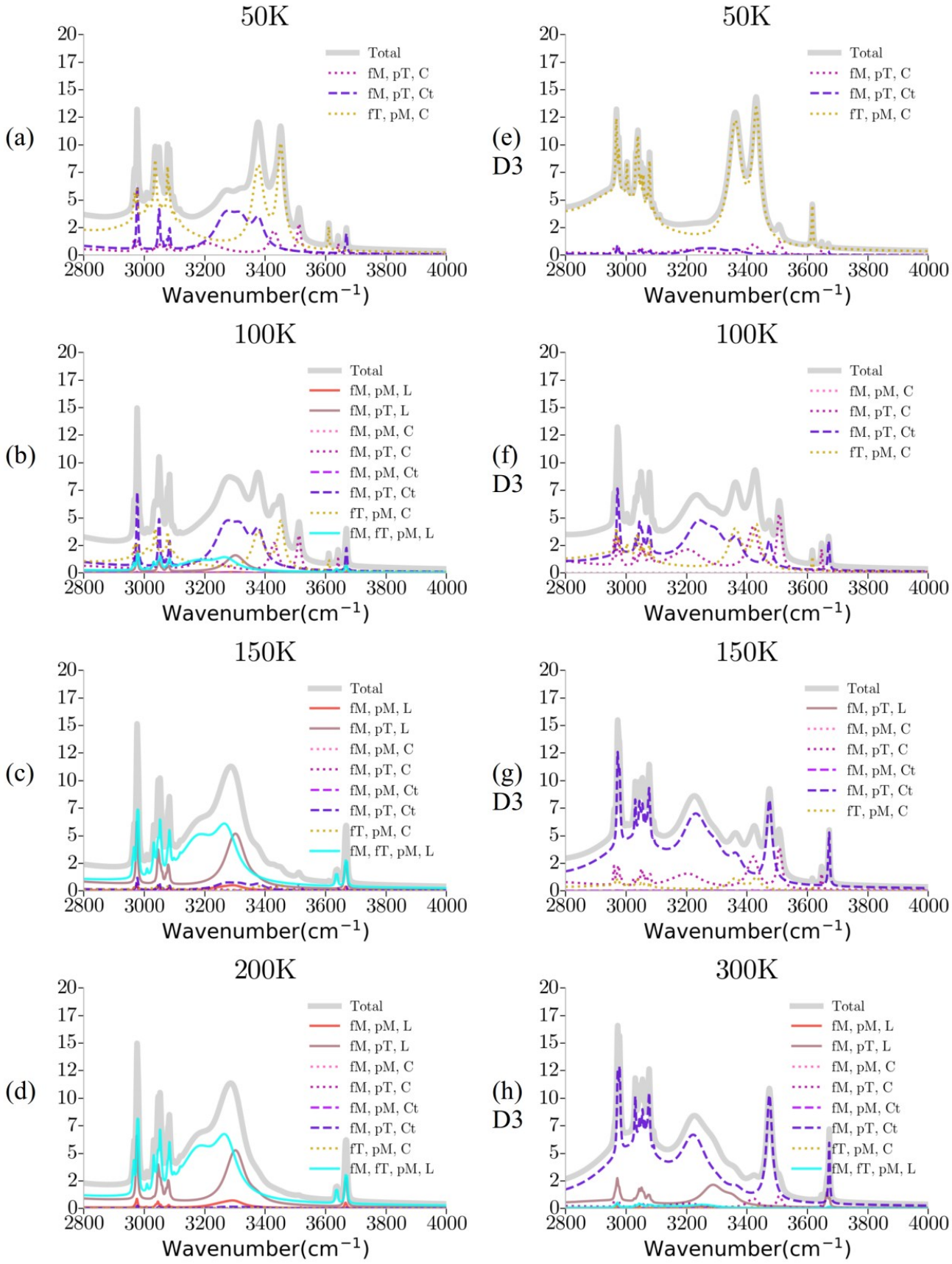

Figure S11 Simulated IR spectra of $H^+(MeOH)_4(t\text{-}BuOH)_1$ using the B3LYP/6-31+G* (a-d) and B3LYP+D3/6-31+G* (e-h) level of theories at various temperatures. The total spectra are marked by grey color. The H-bonded structures are labeled by **L** (linear), **C** (cyclic), and **Ct** (cyclic with a tail) structures. The free OH species and the ion core are labeled by fM (free OH on methanol), fT (free OH on *tert*-butyl alcohol), pM (methanol ion core), and pT (*tert*-butyl alcohol ion core).

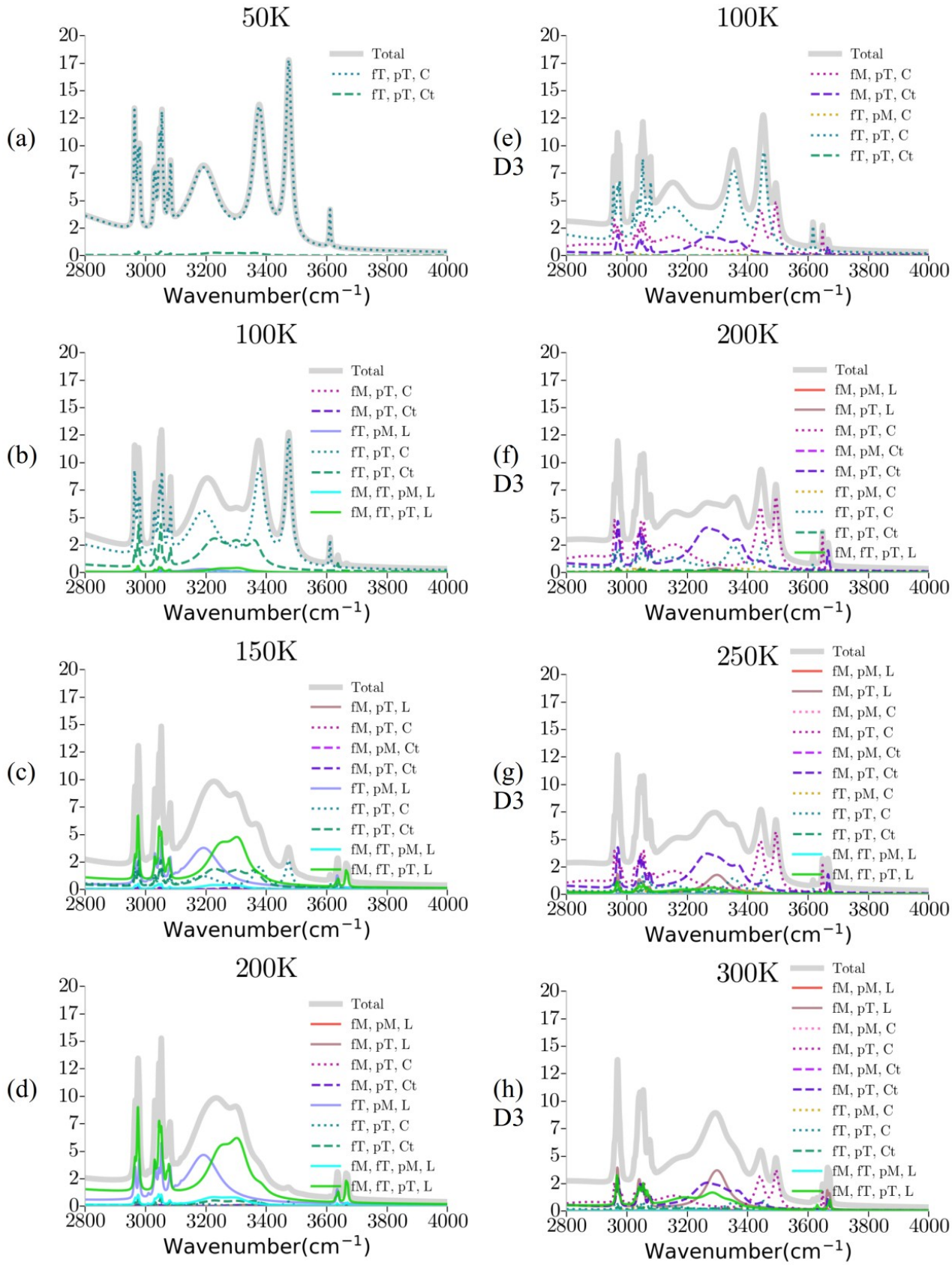

Figure S12 Simulated IR spectra of $H^+(MeOH)_3(t\text{-}BuOH)_2$ using the B3LYP/6-31+G* (a-d) and B3LYP+D3/6-31+G* (e-h) level of theories at various temperatures. The total spectra are marked by grey color. The H-bonded structures are labeled by **L** (linear), **C** (cyclic), and **Ct** (cyclic with a tail) structures. The free OH species and the ion core are labeled by fM (free OH on methanol), fT (free OH on *tert*-butyl alcohol), pM (methanol ion core), and pT (*tert*-butyl alcohol ion core).

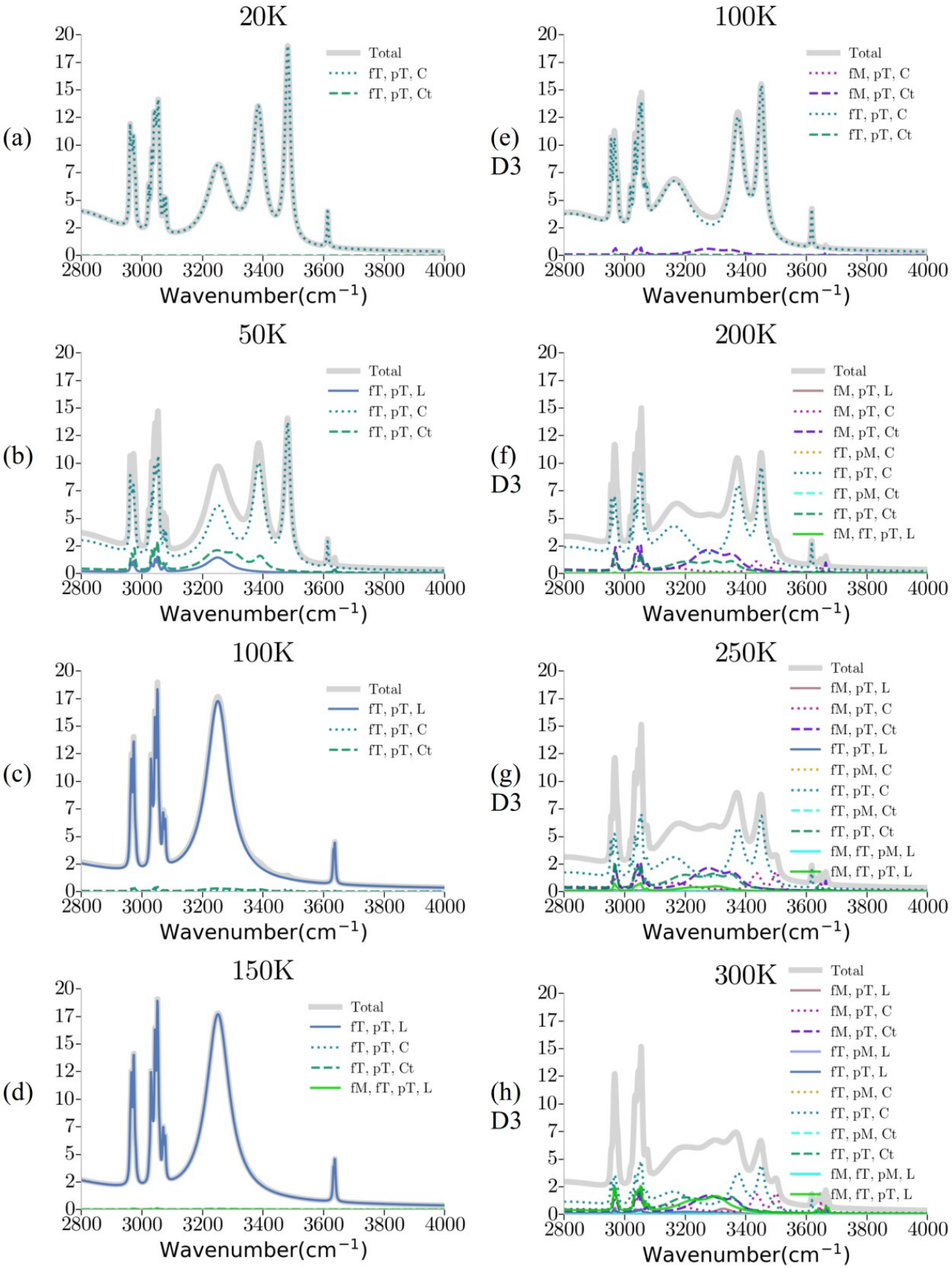

Figure S13 Simulated IR spectra of $H^+(MeOH)_2(t\text{-}BuOH)_3$ using the B3LYP/6-31+G* (a-d) and B3LYP+D3/6-31+G* (e-h) level of theories at various temperatures. The total spectra are marked by grey color. The H-bonded structures are labeled by **L** (linear), **C** (cyclic), and **Ct** (cyclic with a tail) structures. The free OH species and the ion core are labeled by fM (free OH on methanol), fT (free OH on *tert*-butyl alcohol), pM (methanol ion core), and pT (*tert*-butyl alcohol ion core).

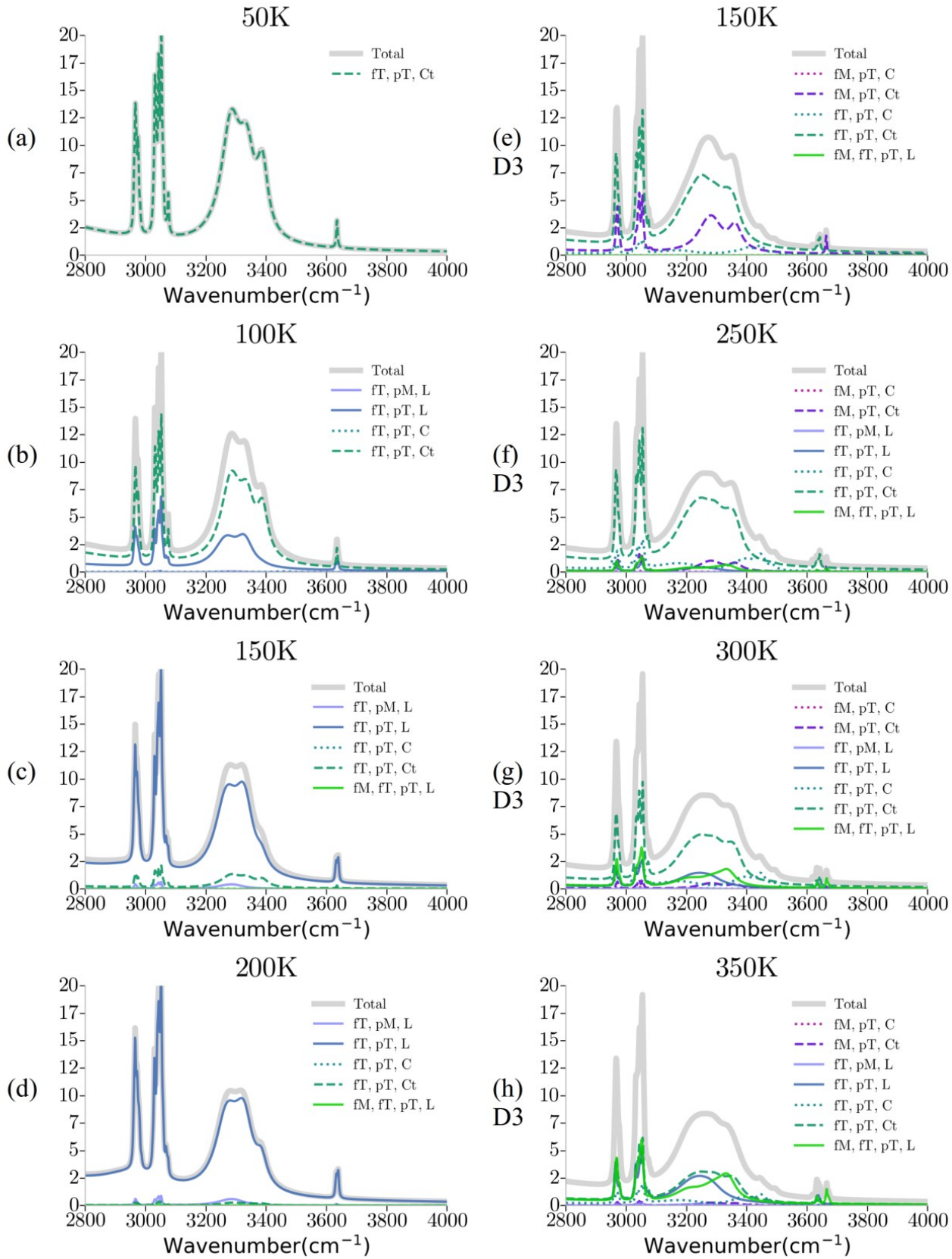

Figure S14 Simulated IR spectra of $H^+(MeOH)_1(t\text{-}BuOH)_4$ using the B3LYP/6-31+G* (a-d) and B3LYP+D3/6-31+G* (e-h) level of theories at various temperatures. The total spectra are marked by grey color. The H-bonded structures are labeled by **L** (linear), **C** (cyclic), and **Ct** (cyclic with a tail) structures. The free OH species and the ion core are labeled by fM (free OH on methanol), fT (free OH on *tert*-butyl alcohol), pM (methanol ion core), and pT (*tert*-butyl alcohol ion core).

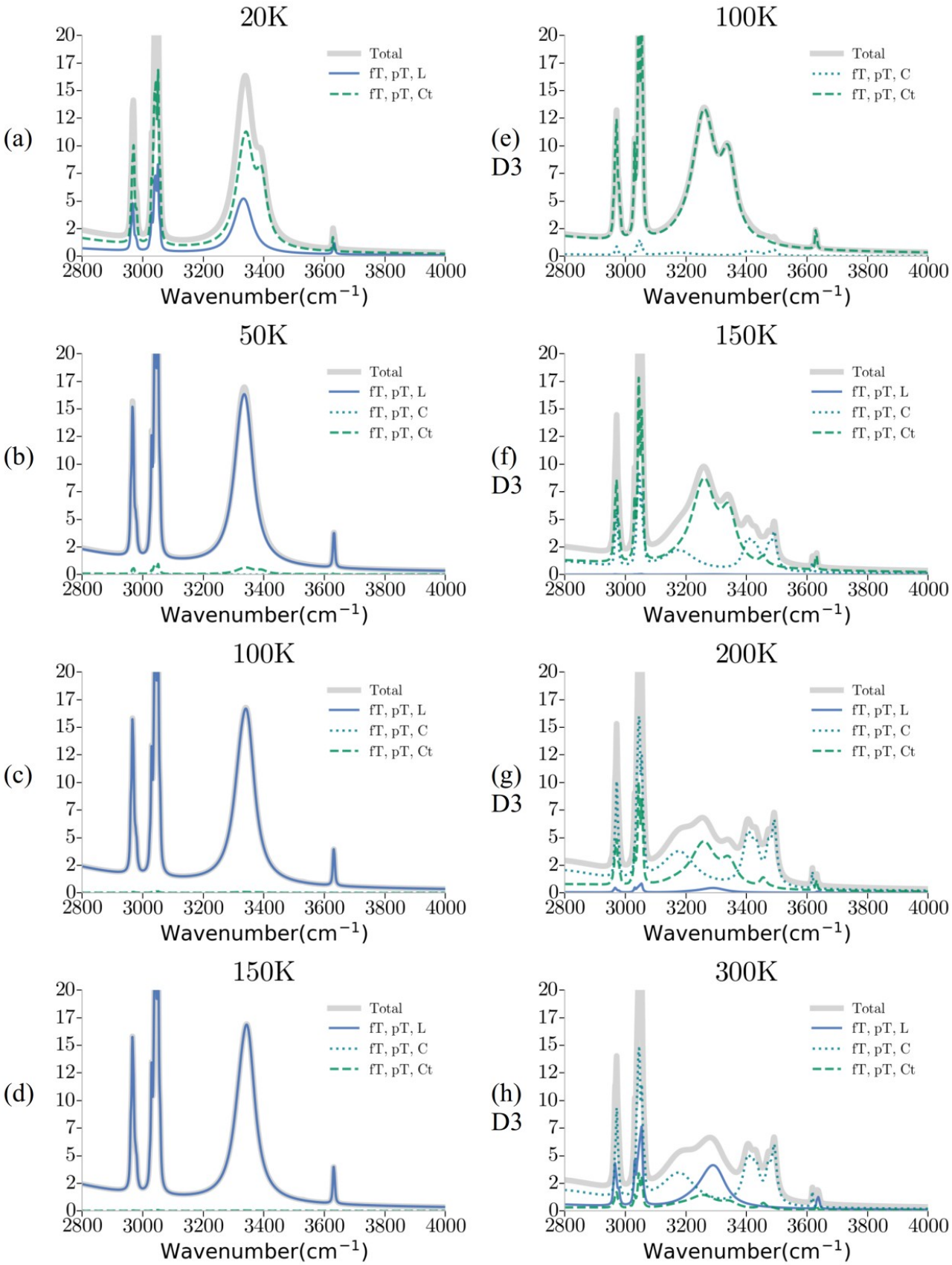

Figure S15 Simulated IR spectra of $H^+(t\text{-BuOH})_5$ using the B3LYP/6-31+G* (a-d) and B3LYP+D3/6-31+G* (e-h) level of theories at various temperatures. The total spectra are marked by grey color. The H-bonded structures are labeled by **L** (linear), **C** (cyclic), and **Ct** (cyclic with a tail) structures. The free OH species and the ion core are labeled by fM (free OH on methanol), fT (free OH on *tert*-butyl alcohol), pM (methanol ion core), and pT (*tert*-butyl alcohol ion core).

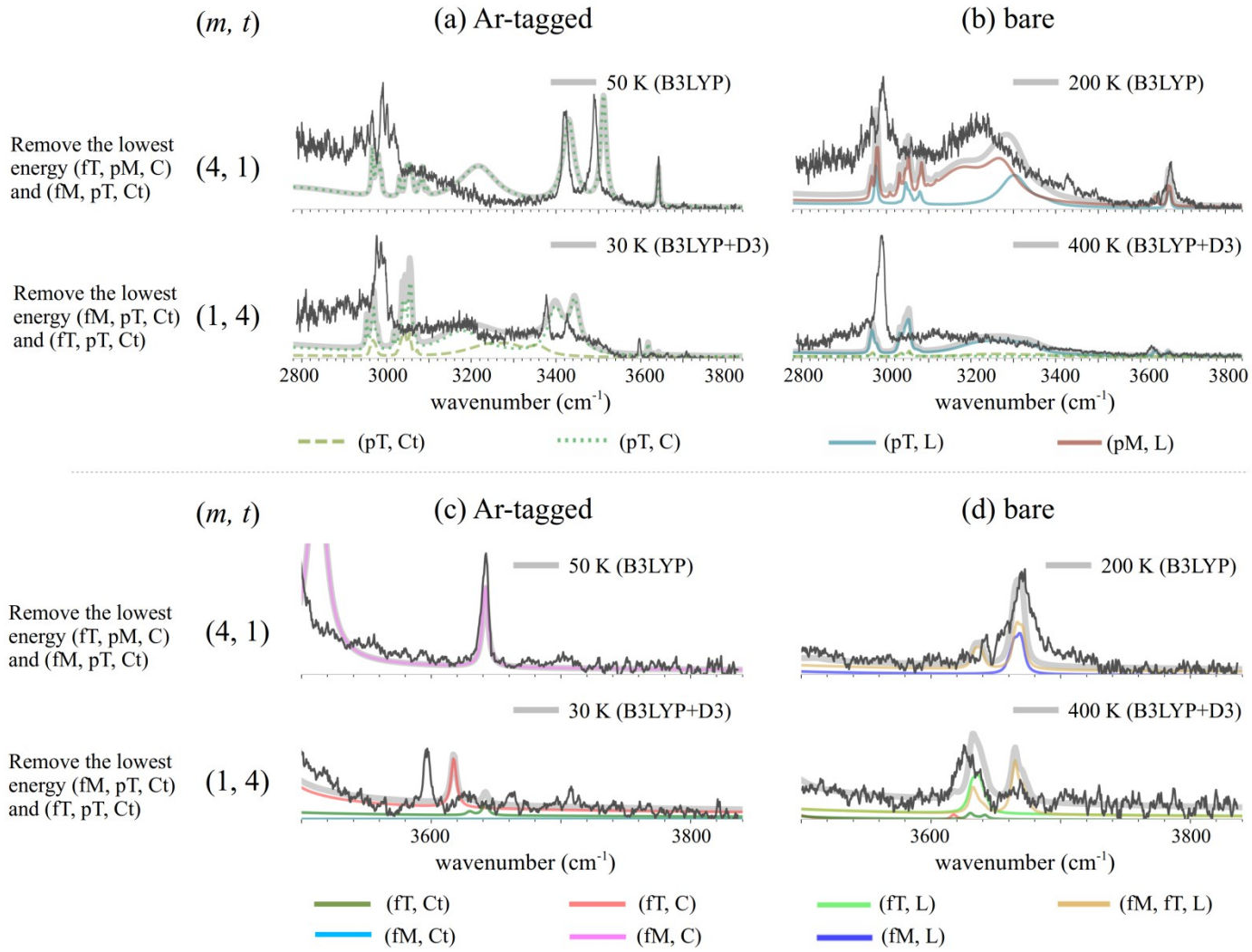

Figure S16 Comparison between the observed IR spectra (black) of Ar-tagged and bare clusters and the Q-HSA simulated IR spectra for $H^+(MeOH)_m(t\text{-BuOH})_t$, (*m, t*) = (4, 1) and (1, 4) by removing the lowest energy structures of (fT, pM, **C**) and (fM, pT, **Ct**) for (4, 1), and (fM, pT, **Ct**) and (fT, pT, **Ct**) for (1, 4). The top figures are the full frequency range spectra (a and b). The bottom figures are the expanded version of the top ones with free OH sites (c and d). The H-bonded structures are labeled by **L** (linear), **C** (cyclic), and **Ct** (cyclic with a tail) structures. The free OH species and the ion core are labeled by fM (free OH on methanol), fT (free OH on *tert*-butyl alcohol), pM (methanol ion core), and pT (*tert*-butyl alcohol ion core).

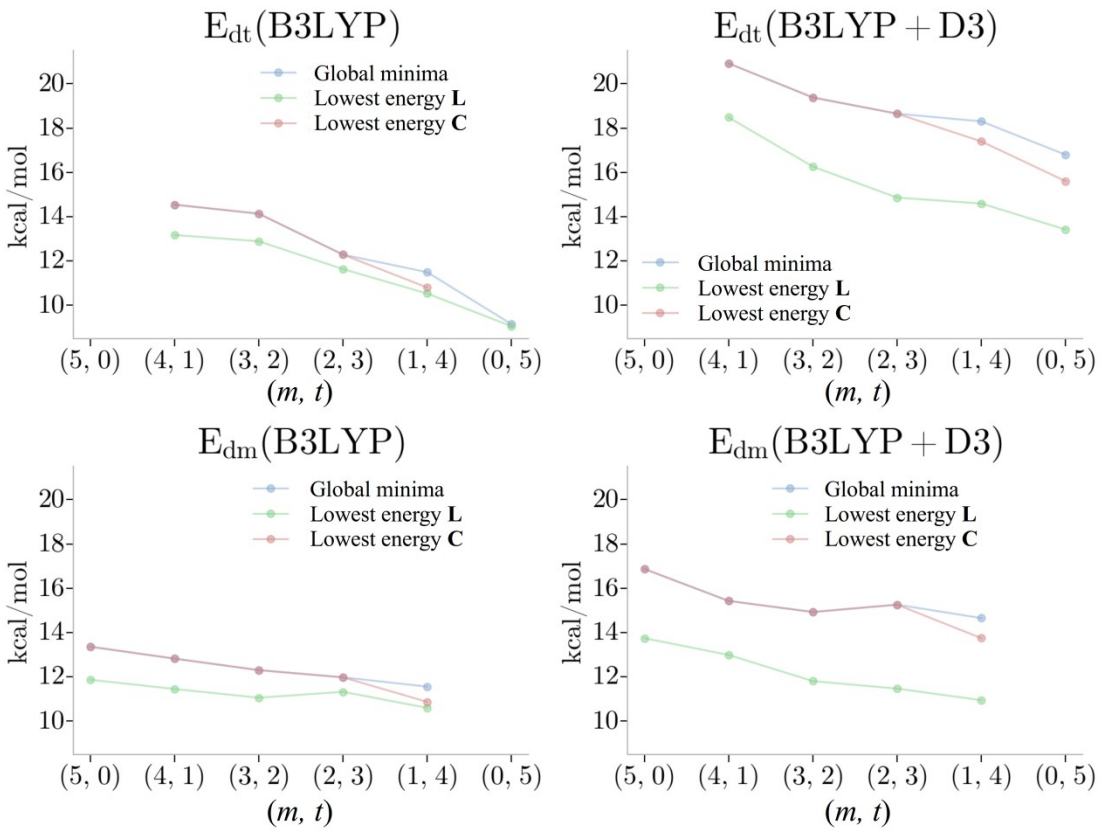

Figure S17 Dissociation energies of $H^+(MeOH)_m(t\text{-BuOH})_t$, $m + t = 5$ clusters. E_{dm} is the dissociation energy to the (m, t) to (m-1, t) channel, and E_{dt} is the dissociation energy for the (m, t) to (m, t-1) channel. Three curves shown in each diagram are for the global minimum isomer (violet), the lowest energy isomer of the **L**-type (green), and the lowest energy isomer of **C**-type cluster (red). Plots are based on the data shown in Tables S6, S8, and S10, in which the dissociation only to the global minimum of $m + t = 4$ in each channel is considered.

Note on the artificial discrimination of specific isomers in dissociation spectroscopy

We have employed dissociation detection to observe the IR spectra. When the dissociation energy of the bare cluster largely depends on its H-bonded structure, artificial discrimination of specific isomer types can occur. For example, if the dissociation energy of a **L** isomer is lower than the one IR photon energy while that of a **C** isomer is higher than the photon energy, selective detection of the L isomer occurs, and the observed isomer population is largely biased. To examine such a possibility, we evaluated the dissociation energies of the different isomer types of the bare clusters of $m + t = 5$. The results are summarized in Figure S17 and Tables S4 - S10. We calculated the dissociation energy only for $m + t = 5$ because of the lack of the comprehensive computational data on $m + t = 3$, which are requested for dissociation energy calculations of $m + t = 4$. However, discussion on $m + t = 5$ is practically enough to examine this issue.

In the calculations, we assumed that the IR predissociation occurs following complete vibrational

energy redistribution (thermalization). Therefore, there would be no clear correlation (restriction) between the H-bond network topology (structures) of the parent and fragment clusters because isomerization would occur prior to dissociation. Then, we focused on the dissociation channels from the global minimum (**C** or **Ct**) and most stable isomers of **L** and **C** of $m + t = 5$, respectively, to the global minimum isomer of $m + t = 4$ (**C** isomers except for the case of $(m, t) = (5, 0)$). In this channel, the lowest dissociation energy is expected for each isomer type of $m + t = 5$.

The results are summarized in Figure S17. We find some clear trends;

1. The dissociation energy of the MeOH-loss channel is lower than that of the *t*-BuOH-loss channel. This is consistent with the experimental observation of the preference of the MeOH-loss channel except for the case of the neat *t*-BuOH cluster ($(m, t) = (0, 5)$).
2. The dissociation energy is evaluated to be higher with the D3 correction.
3. The dissociation energy decreases with the increase of the concentration of *t*-BuOH. The magnitude of dispersion would increase with the increase of the concentration of *t*-BuOH. But the steric repulsion among the bulky *t*-butyl groups also increases, and this would be responsible to the decrease of the dissociation energy.
4. The dissociation energy of the **L** isomer is lower than those of the other (**C** and **Ct**) isomers. The dissociation energy difference is evaluated to be larger with the D3 correction (1-2 kcal/mol without the D3 correction, but 2-3 kcal/mol with the D3 correction). These values simply reflect the energy difference among the parent isomers because the fragment cluster is assumed to be same for the three isomer types.

Item 4 seems to suggest the possibility of the isomer discrimination by the dissociation energy, especially if the energy evaluation with the D3 correction is correct. However, such discrimination would not be effective in the present observations. We focus on the calculated dissociation energies of the MeOH-loss channel with the D3 correction, in which the gap between the dissociation energies of the **L** and **C**/**Ct** isomers is maximum. The calculated lowest dissociation energies of 11~14 kcal/mol of the **L** isomers are actually much higher than the one IR photon energy at the CH stretch region (~8.5 kcal/mol), in which intense bands clearly appear in the observed spectra. This means that the bare clusters should have rich thermal energy which assists the shortage of the IR photon energy to dissociate the cluster (we have confirmed the roughly linear IR power dependence of the fragment signal intensity, and the multiphoton dissociation has been avoided). We have experimentally observed the dissociation of the **L** isomer of (5, 0). This suggests that the thermal energy of the cluster should be larger than 14 - 8.5 = 5.5 kcal/mol. It is reasonable that all the clusters of $m + t = 5$ have roughly the same magnitude of thermal energy because they were produced under the same condition. For (1, 4), the total sum of these thermal and photon energies (14 kcal/mol) is enough to dissociate the **C** isomer, though the sign of the **C** isomer is totally missing in the observed spectrum. Also for (4, 1) ~ (2, 3), the expected total energy (at least ~14 kcal/mol) is close to their dissociation energies of **C**/**Ct** isomers, and sharp cut-off of the dissociation of **C**/**Ct** isomers is hard to consider because of the broad distribution of thermal energy (here, we should note that if we assume ~200 K for the bare clusters, the simulations at B3LYP/D3 predict much larger population of **C**/**Ct** than **L**. Therefore, smaller population of higher thermal energy component, which is requested for dissociation of **C**/**Ct**, can be cancelled by larger isomer population of **C**/**Ct**). The same scenario can be applied to the dissociation

energy evaluation without the D3 correction.

Based on the discussion described above, we conclude that the artificial discrimination of specific isomers would not occurs in the present observations. The unexpected high temperature requested to reproduce some of the observed isomer populations of the bare clusters with the DFT computations should be attributed to the problem of the accuracy of the DFT energy evaluation, not to the artificial isomer discrimination.